Geodesy and Geodynamics 2013,4(4):17-25

http://www.jgg09.com
Doi:10.3724/SP.J.1246.2013.04017

Correlation between seismicity and geomorphology in Dingxi Basin, Gansu Province, China

Li Xue[1,2], Liu Xiaoli[1,2], Li Jinggang[1,2], Zhang Lifen[1,2], Wang Qiuliang[1,2] and Liao Wulin[1,2]

[1] *Key Laboratory of Earthquake Geodesy, Institute of Seismology, China Earthquake Administration, Wuhan* 430071, *China*

[2] *Wuhan Base of Institute of Crustal Geodynamics, China Earthquake Administration, Wuhan* 430071, *China*

Abstract: A *M*6.6 earthquake occurred on July 22, 2013 at Dingxi Basin in Gansu Province within the tectonially expanding northeastern margin of the Qinghai-Tibet Plateau. We analyzed the geomorphological features of the Dingxi Basin by using remote sensing technology and compared them with local seismic activity. We found that most of the river basins are at the robust stage of development and that the major local rivers and the development of some basins boundaries are controlled by the seismic faults. Among four zones identified to have significant tectonic activities, the northwestly-oriented one located in the south has the highest seismic activity, and it is where the *M*6.6 earthquake occurrred.

Key words: Dingxi Basin; geomorphology; hypsometric integral; stream length-gradient; seismic activity

1 Introduction

The Qinghai-Tibet Plateau, which is caused by the collision of Indian plate with Eurasian plate, has continued to expand and grow since Cenozoic time, and the northeastern margin of the plateau is considered to be a frontier of the expansion[1]. A *M*6.6 earthquake occurred on July 22,2013, with epicenter located between the counties of Minxian and Zhangxian at Dingxi Basin of Gansu Province in this margin. In this study we tried to investigate the relationship between the local seismic activities and the basins' geomorphological features.

The geomorphological features were studied by remote sensing technology and a digital elevation model (DEM), both of which have been used as tools for the study of plateau uplift and orogenic evolution[2]. The analysis of river geomorphology features may help understand the status of a regional tectonic activity. To facilitate such studies, Strahler[3,4] designed a hypsometric integral to quantitatively analyze the impact of tectonic activity and erosion on the basins. Also, Hack[5] proposed a river longitudinal logarithmic plot and stream length-gradient (SL) index for studying the influence of lithology and tectonic activity on stream length-gradient data.

Received:2013-08-01; Acceptd:2013-09-08

Corresponding author:Li Xue, E-mail:leexue1211@126.com

This work is supported by the Director Foundation of the Institute of Seismology, China Earthquake Administration (201116002, 201056076)

2 Overview of the study area

Dingxi Basin covers one district (An'ding) and six counties: Lintao, Weiyuan, Longxi, Tongwei, Zhangxian and Minxian, with elevation ranging from 1640 m to 3900 m (Fig. 1). Dingxi Basin is divided by the Weihe river into two parts: A loess plateau in the north and a chilly and humid region of high-elevation in the south. Other main rivers in Dingxi Basin include Taohe, Pangshahe, Xianhe.

3 Analysis

3.1 Extraction of river and basin

To analyze the topography, we used ASTER GDEM,

which has a 30 m horizontal and a 20 m vertical precision, as a data source. After filling low-lying land and calculating the flow direction and accumulation, we extracted the river networks. From the Strahler grade of the river networks and the GIS data announced by National Fundamental Geographic Information System (NFGIS), 33 major rivers were identified as R1 to R33. According to the river networks and flow direction, watershed segmentation was employed to get the basins of each river. According to the merging of basins, 11 river basins were obtained (B1 to B11). The distribution of the rivers and basins are shown in figure 2 and table 1.

3.2 Hypsometric integral

Total elevation (H) is relief within basin (maximum elevation minus the minimum elevation), total area (A) is total surface area of basin, and area (a) is surface area within basin above a given altitude (h).

The hypsometric integral curves of the 11 basins (Fig. 3) are mostly concave in shape, especially B1 and B4, but B6 to B11 are relatively flat. Such curvature indicates the degree to which the basin is affected by tectonic uplift and erosion[6].

As a measure of developmental stage, the Hypsometric integral (HI) of basins is calculated by[7]:

$$HI=\frac{H_{mean}-H_{min}}{H_{max}-H_{min}} \quad (1)$$

where H_{mean}, H_{min} and H_{max} are, respectively, mean, minimum, and maximum of basin elevation. Table 2 shows the calculated parameters of the basins[8]. The influences of tectonic uplift and erosion are different at different basin-developmental stages; uplift dominates at a young stage, erosion dominates at an old stage, and they balance each other at a robust stage[9].

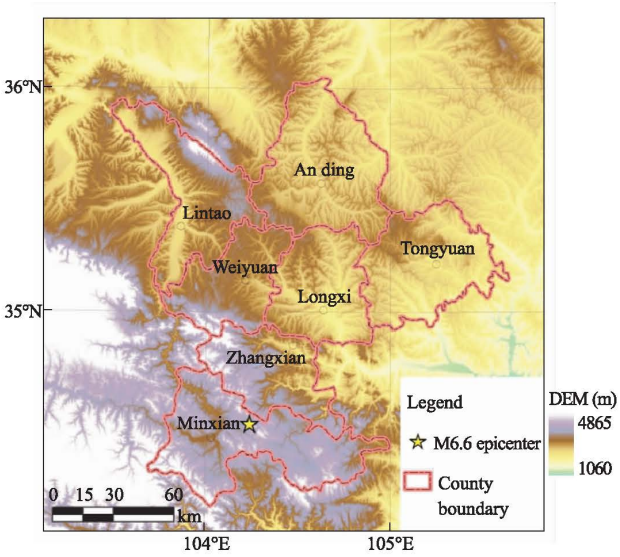

Figure 1 Digital elevation model of Dingxi Basin

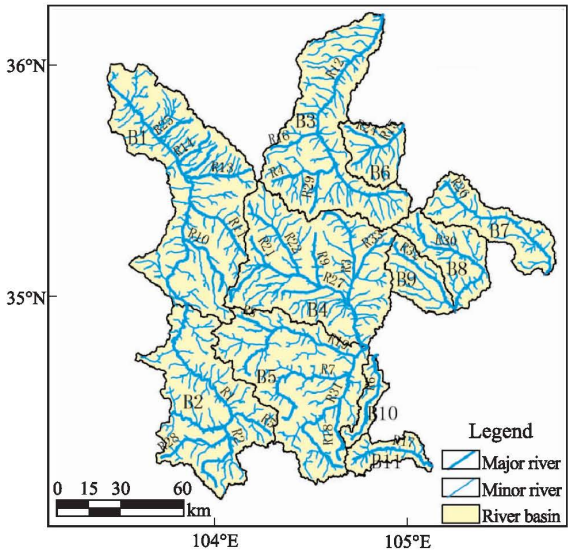

Figure 2 Rivers and basins of the study area

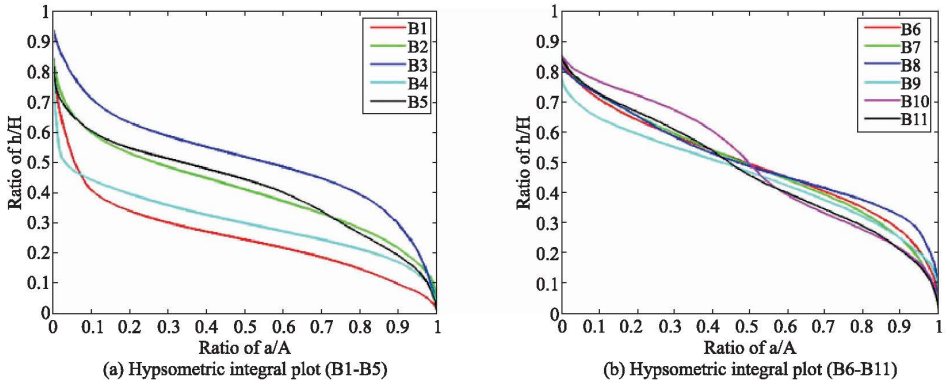

(a) Hypsometric integral plot (B1-B5) (b) Hypsometric integral plot (B6-B11)

Figure 3 Hypsometric integral plot

Table 1 Corresponding relation between rivers and basins

Basin No.	River No.	River names	Basin No.	River No.	River names
B1	R1(lower)	Taohe lower reaches	B4	R21	Cuijiahe
	R10			R22	Xianhe
	R13			R27	Weihe
	R23	Haoshuigou		R33	
	R25		B5	R7	
B2	R1(upper)	Taohe middle reaches		R8	Tiegouhe
	R2			R18	Nabudahe
	R5	Nanahe		R19	Zhanghe
	R28	Xihe		R31	
B3	R4		B6	R15	
	R12	Guanchuanhe		R24	
	R16		B7	R26	
	R29		B8	R30	Niuguhe
B4	R3		B9	R32	Kushuihe
	R9		B10	R6	Nanhe
	R20	Keyanghe	B11	R17	Yanzihe

Table 2 Topographic parameters of the basins

Basin No.	Elevation(m)			Area (km^2)	*HI*	Developmental stage
	Min	Max	Difference			
B1	1 708	3 920	2 212	4 531.7	0.256 2	old (robust)
B2	2 024	3 895	1 871	3 103.2	0.409 6	robust(old)
B3	1 520	2 569	1 049	3 507.9	0.510 8	robust
B4	1 539	3 477	1 938	3 999.2	0.303 4	old (robust)
B5	1 534	3 921	2 387	3 602.6	0.417 5	robust(old)
B6	1 661	2 333	672	746.5	0.496 3	robust
B7	1 331	2 398	1 067	1 249.2	0.492 2	robust
B8	1 379	2 525	1 146	1 092.9	0.506 8	robust
B9	1 412	2 439	1 027	717.5	0.461 9	robust
B10	1 485	3 117	1 632	361.6	0.498 5	robust
B11	1 455	3 270	1 815	485.3	0.474 2	robust

3.3 Stream length-gradient

Hack represents river longitudinal profile by the logarithmic equation[10].

$$H = c - K \log L \tag{2}$$

where H represents the elevation of the river, c is a constant, the so-called "equilibrium gradient index" K indicates the slope of the profile curve, and L represents the distance from the river source to the basin outlet. The stream length-gradient (SL) index is calculated by[10].

$$SL = (\Delta H / \Delta L)\bar{L} \tag{3}$$

ΔH represents the elevation difference of unit river section, ΔL is the distance of the unit river section (set to 1km in this study), $\bar{L}$ represents the distance from the river source to the midpoint of the river section. There is a close relationship between SL and erosion resistance of bedrocks. An abnormal SL peak in the same bedrock reflects the impact of recent tectonic activity on the development of the river[11].

Figure 4 shows the calculated Hack profiles of the major rivers in Dingxi Basin. All curves are convex to different degrees. Table 3 lists the calculated geomor-

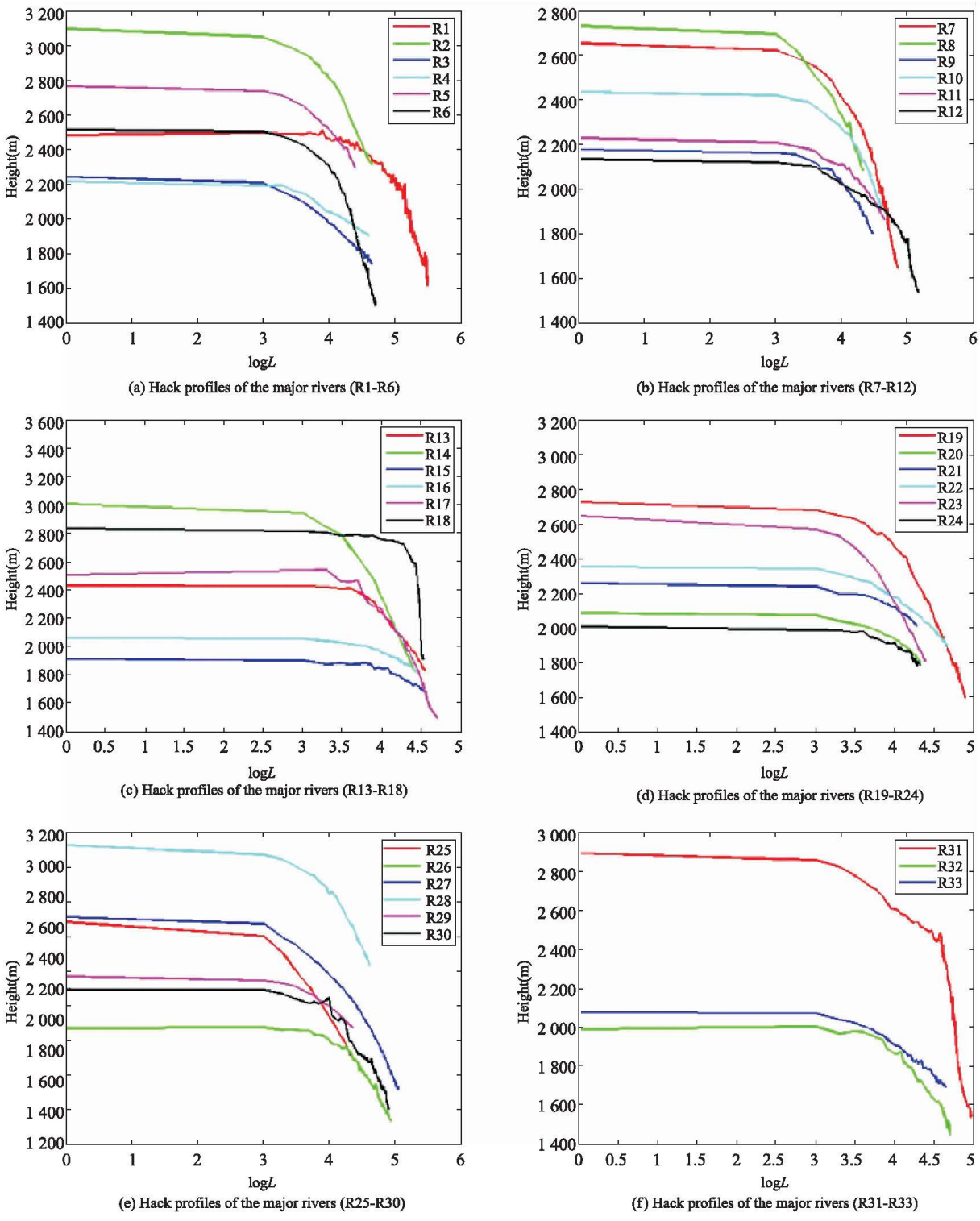

(a) Hack profiles of the major rivers (R1-R6)

(b) Hack profiles of the major rivers (R7-R12)

(c) Hack profiles of the major rivers (R13-R18)

(d) Hack profiles of the major rivers (R19-R24)

(e) Hack profiles of the major rivers (R25-R30)

(f) Hack profiles of the major rivers (R31-R33)

Figure 4 Hack profiles of the major rivers

phological parameters of the major rivers.

Because of the difference in river length, the *SL* indexes of the major rivers are difficult to compare. Thus we have used the *SL/K* index, which is the standardization of *SL*, to identify the abnormal river sections (any value bigger than 5)[5]. Table 4 shows the statistics of abnormal sections.

As shown in table 4, there are 8 rivers with an abnormal rate greater than 0.2: R1, R12, R15, R18, R24, R26, R30, R31. Figure 5 is a *SL/K* line chart of the abnormal rivers. Figures 5 and 6 show that the identified abnormal sections are not concentrated near

the stratigraphic boundaries (dashed lines), but are distributed mostly in the same bedrocks, indicating that the impact of tectonic uplift is greater than that of lithological changes.

The abnormal river sections indicate the impact of the tectonic uplifts, which intersect the rivers approximately vertically. In this way, we identified four zones of relatively strong tectonic activity (Fig. 6): The northwestly-oriented Zone 1 and 4, the noth-northwestly-oriented Zone 2, and the northeastly-oriented Zone 3.

Table 3 Geomorphologic parameters of the major rivers

River No.	Length (km)	Elevation(m)			*K*	River No.	Length (km)	Elevation(m)			*K*
		Source	Outlet	Difference				Source	Outlet	Difference	
R1	318.1	2475	1658	817	148.5	R18	33.7	2827	1902	925	204.3
R2	46.8	3090	2311	779	166.8	R19	78.6	2721	1591	1130	230.8
R3	45.4	2236	1736	500	107.4	R20	21.4	2081	1796	285	65.8
R4	40.5	2208	1891	317	68.8	R21	19.0	2252	2007	245	57.3
R5	25.6	2760	2285	475	107.8	R22	47.6	2345	1879	466	99.6
R6	51.6	2507	1492	1015	215.4	R23	25.1	2641	1810	831	188.9
R7	70.8	2650	1639	1011	208.4	R24	21.8	2002	1780	222	51.2
R8	21.3	2728	2079	649	150.0	R25	22.3	2624	1764	860	197.8
R9	29.4	2172	1796	376	84.2	R26	87.8	1939	1344	595	120.4
R10	39.7	2430	1910	520	113.1	R27	111.6	2654	1563	1091	216.1
R11	44.6	2224	1857	367	78.9	R28	42.3	3118	2342	776	167.7
R12	146.6	2129	1530	599	115.9	R29	23.9	2271	1941	330	75.4
R13	36.2	2423	1821	602	132.1	R30	80.9	2186	1421	765	155.9
R14	27.2	2999	1815	1184	267.0	R31	95.6	2892	1547	1345	270.0
R15	35.1	1906	1673	233	51.3	R32	50.9	1987	1441	546	116.0
R16	26.4	2054	1827	227	51.3	R33	45.2	2072	1690	382	82.1
R17	51.7	2497	1487	1010	214.3						

Table 4 Abnormal *SL/K* statistics of the major rivers

River No.	Number of sections	Number of abnormal sections (*SL/K*>5)	Abnormal rate	River No.	Number of sections	Number of abnormal sections (*SL/K*>5)	Abnormal rate
R1	319	153	0.479 6	R18	34	7	0.205 9
R2	47	1	0.021 3	R19	79	6	0.075 9
R3	45	6	0.133 3	R20	22	0	0
R4	41	1	0.024 4	R21	20	2	0.100 0
R5	26	2	0.076 9	R22	48	3	0.062 5
R6	52	2	0.038 5	R23	26	0	0
R7	71	7	0.098 6	R24	22	6	0.272 7
R8	22	1	0.045 5	R25	23	0	0
R9	30	3	0.100 0	R26	88	24	0.272 7
R10	40	3	0.075 0	R27	112	5	0.044 6
R11	45	2	0.044 4	R28	43	1	0.023 3
R12	147	39	0.265 3	R29	24	0	0
R13	37	1	0.027 0	R30	81	18	0.222 2
R14	28	0	0	R31	96	21	0.218 8
R15	36	10	0.277 8	R32	51	9	0.176 5
R16	27	5	0.185 2	R33	46	9	0.195 7
R17	52	4	0.076 9				

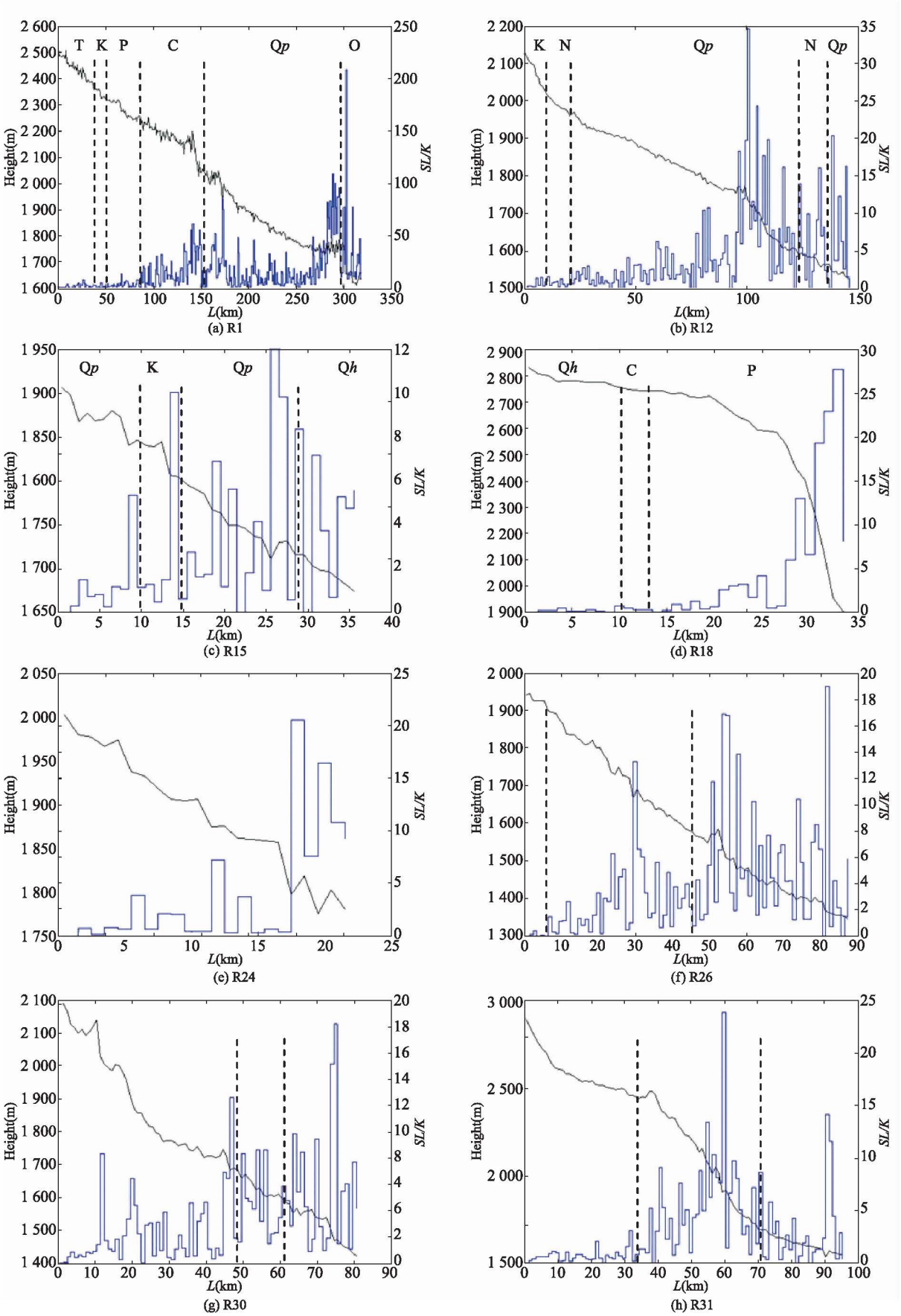

Figure 5 *SL* and *SL/K* lines of the abnormal rivers

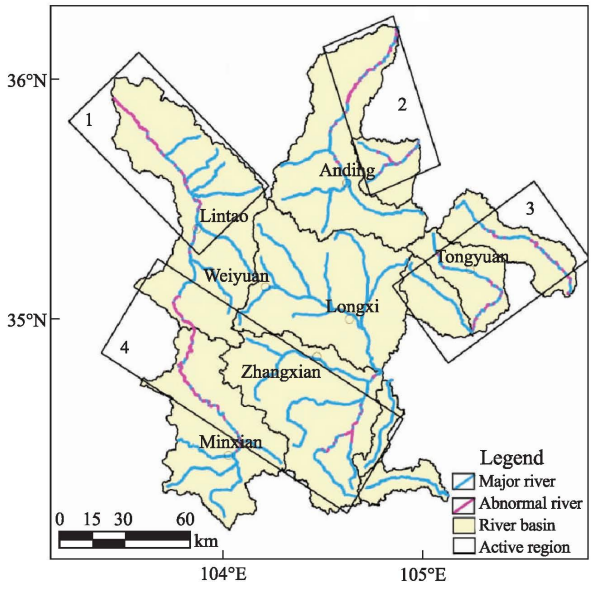

Figure 6 Distribution of abnormal river sections

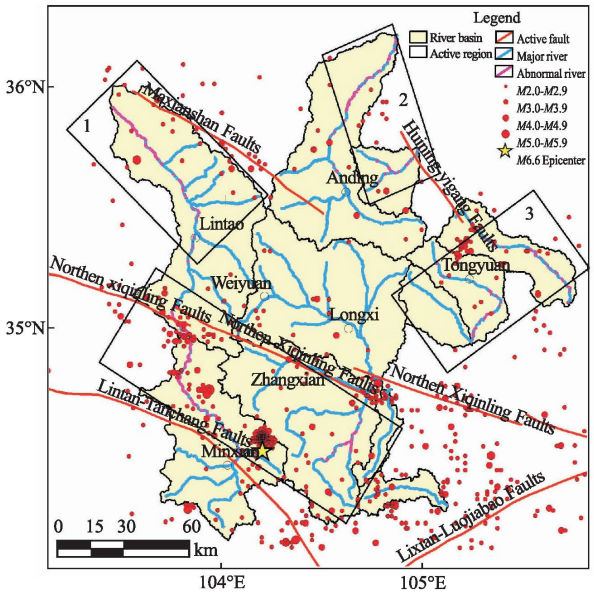

Figure 7 Distribution of abnormal sections, earthquakes, and active faults

3.4 Geomorphological features and seismic activity

To study the correlation between geomorphological features and local seismicity, we superimposed on figure 6 the distributions of active faults according to Deng Qidong and 399 earthquakes of $M>2$ since 1965 according to China Earthquake Networks Center. As shown in figure 7, most of the earthquakes occurred in a triangular southern region bordered by the Northern Xiqinling, Lintan-Tanchang, and Lixian-Luojiabao Faults.

We divided the period since 1965 into 10 five-year sections, in which the statistics of earthquake number and average magnitude of each basin. As shown in figure 8(a), the number of earthquakes in B1, B2, B5 and B7 are greater than in other basins; the number of earthquakes tend to increase with time in B2 and B5, remain stable in B1 and B7, and show cyclical changes in B3. Figure 8(b) shows that the average magnitude was gradually increasing in B2, but was relatively stable elsewhere.

As shown in figure 7, the spatial distribution of earthquakes in the study area is clustered. We calculated the distance between earthquake epicenter and basin boundary, and show the statistics in figure 9. The result indicates that 68.3% of the earthquakes occurred within 4.7 km of a basin boundary, and 95% within 11.4 km.

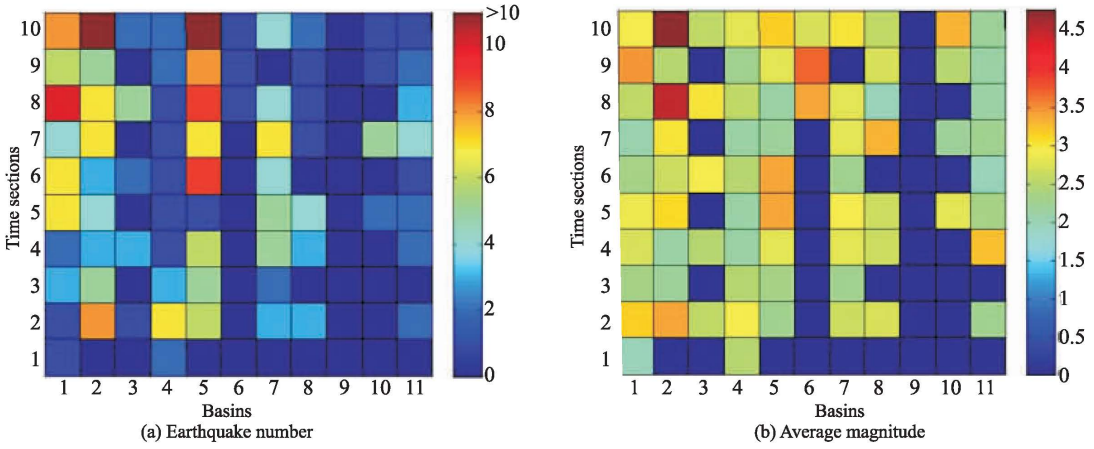

Figure 8 Statistics of earthquake number and average magnitude in different time sections and basins

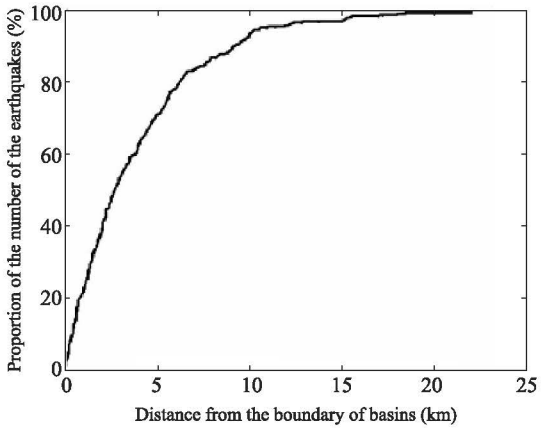

Figure 9 Statistical distribution of distance of earthquake epicenter to basin boundary

3.5 Discussion

Our result suggests that B1 and B4 are old and the other basins are robust in their evolution stages. Historical earthquakes in Dingxi Basin are mainly concentrated in B1, B2, B5 and B7, but *HI* values of these basins are not significant different from other basins. Thus the seismic activity does not appear to be related to the development stages of these basins.

On the other hand, the development of these basin boundaries seems to be controlled by earthquake-related active faults. This is seen from the distribution of basins and active faults: Northern Xiqinling Faults cross the junction of B1 and B2 as well as B5 and B10, Lintan-Tanchang Faults cross B2, Huining-Yigang Faults cross B6 and B7. The earthquake-concentration areas are northeastern margin of B1, southern margin of B11, and the junction of B1 and B2, B2 and B5, B4 and B5, B5 and B10, as well as B7 and B8.

The abnormal sections of some major rivers appear to be controlled by active faults also. Figure 7 shows four zones in which the distribution of abnormal sections is generally consistent with the distribution of active faults, but with some local differences. Both Northern Xiqinling Faults and Lintan-Tanchang Faults are in the NW direction. The abnormal sections in Zone 4 intersect with both faults and the fold belts between the faults at a large angle, indicateing that these two faults have exercised control in Zone 4. Similarly, Zone 2 is controlled by Huining-Yigang Faults. There is no such fault in Zone 1 and Zone 3, however. We inferred that the abnormal sections in these Zones may be controlled by some buried faults or secondary faults. The analysis of stream length-gradient shows that this index too is sensitively controlled by tectonic activity.

The *M*6.6 Dingxi earthquake is the largest event since 1965 in the study area, and it is located in Zone 4, which has been seismically active in the past. The seismic activity has been less active in Zone 3 and infrequent in Zone 1 and Zone 2. Thus the tectonic activity in the southern part of the study area is stronger than other parts.

4 Conclusion

In this study, we have analyzed the geomorphological features of Dingxi basins by using the remote sensing technology and compared them with the regional seismic and geological background. We found that:

1) Most basins in study area are in the robust developmental stage, and some basins are controlled by active faults.

2) The stream length-gradients are impacted more by tectonic activity than lithology changes.

3) Four zones have significant tectonic activities, which is consistent with the distribution analysis of historical earthquakes and abnormal river sections. The northwesternly-oriented southern Zone 4 has the highest activity, and is where the *M*6.6 Dingxi earthquake occurred.

References

[1] Zhang Peizhen, Zheng Dewen, Yin Gongming, et al. Discussion on late Cenozoic growth and rise of northeastern margin of the Tibetan Plateau. Quaternary Sciences, 2006, 26(1): 5-13. (in Chinese)

[2] Zhang Huiping, Yang Nong, Liu Shaofeng, et al. Recent progress in the DEM-based tectonogeomorphic study. Geological Bulletin of China, 2006, 25(6):660-669. (in Chinese)

[3] Kale V S and Shejwalkar N. Uplift along the western margin of the Deccan Basalt Province: Is there any geomorphometric evidence. Journal of Earth System Science, 2008, 117(6):959-971.

[4] Chen Yanjie. Morphotectonic features of taiwan mountain belt based on hypsometric integral, Topographic Fractals and SL Index. Taiwan: National Cheng Gong University, 2004. (in Chinese)

[5] Ji Yapeng, Gao Hongshan, Pan Baotian, et al. Implication of

active structure in the upper reaches of Weihe river basin from stream length-gradient index (SL index) and Hack profile. Journal of Lanzhou University (Natural Sciences), 2011, 47(4): 1-6. (in Chinese)

[6] Xin Zhongbao, Xu Jiongxin and Ma Yuanxu. Hypsometric integral analysis and its sediment yield implications in the Loess Plateau, China. Journal of Mountain Science, 2008, 26(3): 356-363. (in Chinese)

[7] Li Zongmeng, Gao Hongshan, Pan Baotian, et al. Geomorphic indices of the river and drainage in Helan Mountain and its indication to tectonics. Arid Land Geography, 2012, 35(3): 422-429. (in Chinese)

[8] Jiang Luguang and Zhang Zulu. Altitude-area analysis on the drainage landform in the Luzhongnan mountainous region. Journal of Shandong Normal University (Natural Science), 2003, 18(1): 63-66. (in Chinese)

[9] Zhang Jingchun, Li Chuanchuan, Zhang Mei, et al. Geomorphologic analysis of the Golumd river drainage basin based on hypsometric integral value. Journal of Mountain Science, 2011, 29(3): 257-268. (in Chinese)

[10] Zhao Hongzhuang, Li Youli and Yang Jingchun. Implication of active structure along the northern Tianshan by stream length-gradient index and hack profile. Acta Scientiarum Naturalium Universitatis Pekinensis, 2010, 46(2): 237-244. (in Chinese)

[11] Qian Cheng, Han Jianen, Zhu Dagang, et al. An analysis of geomorphologic characteristics of the Yellow River source region based on ASTER-GDEM. Geology in China, 2012, 39(5): 1247-1260. (in Chinese)